

Transformation Coding: Simple Objectives for Equivariant Representations

Mehran Shakerinava^{*1,2} Arnab Kumar Mondal^{*1,2} Siamak Ravanbakhsh^{1,2}

Abstract

We present a simple non-generative approach to deep representation learning that seeks equivariant deep embedding through simple objectives. In contrast to existing equivariant networks, our transformation coding approach does not constrain the choice of the feed-forward layer or the architecture and allows for an unknown group action on the input space. We introduce several such transformation coding objectives for different Lie groups such as the Euclidean, Orthogonal and the Unitary groups. When using product groups, the representation is decomposed and disentangled. We show that the presence of additional information on different transformations improves disentanglement in transformation coding. We evaluate the representations learnt by transformation coding both qualitatively and quantitatively on downstream tasks, including reinforcement learning.

1. Introduction

Sample efficient representation learning is a key open challenge in deep learning for AI. Despite their success in many settings, generative representations are generally deemed sample inefficient. Therefore interest in self-supervision and contrastive learning techniques has significantly increased over the past few years. While contrastive learning objectives often create *invariance* to certain (symmetry) transformations, in this paper, we pursue alternative objectives toward *equivariant* representations.

In contrast to previous equivariant networks, our approach, called *transformation coding*, does not require any specialized architecture, and it can accommodate any non-linear transformation of the input. More importantly, one does not even need to know the correspondence between the transformations of the data and the underlying abstract group. For example, if our data consists of images before and after

^{*}Equal contribution ¹School of Computer Science, McGill University, Montréal, Canada ²Mila- Quebec Artificial Intelligence Institute, Montréal, Canada. Correspondence to: Arnab Kumar Mondal <arnab.mondal@mila.quebec>.

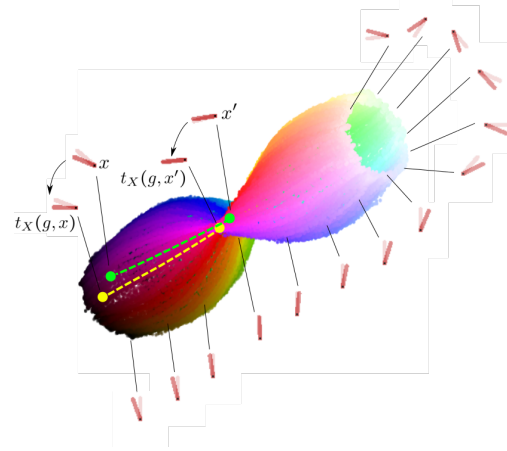


Figure 1. The $E(3)$ -equivariant embedding for the pendulum. The input x consists of a pair of images that together identify both the location and the velocity of a pendulum. The learned equivariant embedding encodes both the location (change of color) and velocity (change of brightness). The two circular ends (black and white) correspond to states of maximum velocity in opposite directions. The transformation coding objective for the *Euclidean group* learns this embedding by preserving the pairwise distance between the codes before $(f(x), f(x'))$ and after $(f(t_X(g, x)), f(t_X(g, x')))$ transformations of the input by t_X . For the pendulum, the transformations are in the form of positive or negative torque in some range. For yellow and green blobs on the manifold, the torque is applied clockwise.

changing the camera angle, we do not need to know the actual angle. However, for example, we may need pairs of images in which the camera angle changes by the same amount.

In the following, first, we observe that equivariance, in general, is a very weak inductive bias. In particular, we show that an injective code is equivariant to “any” transformation group. However, in this manifestation of equivariance, the group action on the code can be highly non-linear. Since the simplicity of the action on the latent space seems essential for equivariance to become a useful learning bias, we *regularize* the group action on the code to make it “simple”. This *symmetry regularization* objective is group-dependent and the essence of our approach to transformation-based coding.

Our symmetry objectives rely on the idea that the transfor-

mation groups preserve specific quantities. For example, the defining action of the Euclidean group preserves the Euclidean distance, and all Euclidean distance preserving transformations are of this form. Therefore, to enforce equivariance to the Euclidean group, it is sufficient to ensure that the embedding of any two data points has the same distance before and after the same transformation of the inputs; see Figure 1. We present similar objectives for several other groups. Transformation coding combines this simple recipe with an injectivity constraint to produce equivariant representations without the need for a reconstruction loss or a hard constraint on the deep architecture.

2. Related Works

Finding effective priors and objectives for deep representation learning is an integral part of the quest for AI (Bengio et al., 2013). Recent years have witnessed a growing interest in self-supervision and, in particular, contrastive objectives (Hadsell et al., 2006; Oord et al., 2018; Chen et al., 2020; Tian et al., 2019; He et al., 2020; Zbontar et al., 2021; Ermolov et al., 2021). While the use of transformations is prominent in these works, in many settings the objective encourages *invariance* to certain transformations, making such models useful for invariant downstream tasks such as classification. Similar to many of these methods, we also use transformed pairs to learn a representation, with the distinction of learning an *equivariant* representation.

Learning both invariant and equivariant deep representations has been the subject of many works over the past decade. Many recent efforts in this direction have focused on the design of equivariant maps (Wood & Shawe-Taylor, 1996; Cohen & Welling, 2016; Ravanbakhsh et al., 2017; Kondor & Trivedi, 2018; Cohen et al., 2019; Finzi et al., 2021; Villar et al., 2021) where the “linear” action of the group on the data is known. Due to this constraint, the application of these models has been focused on fixed geometric data such as images, sets, graphs, and spherical data, or physically motivated Poincare group, among others.

In the present work, the group action is unknown and possibly non-linear. Therefore, in contrast to many prior work, linear representation theory plays no significant role. Our setup is closer to the body of work on generative representation learning (Burgess et al., 2018; Chen et al., 2016; Mita et al., 2021), in which the (linear) transformation is applied to the latent space (Quessard et al., 2020; Worrall et al., 2017; Kulkarni et al., 2015; Lenc & Vedaldi, 2016; Cohen & Welling, 2014; Falorsi et al., 2018). Among these generative coding methods, transforming autoencoder (Hinton et al., 2011) is a closely related early work that, in addition to equivariance, seeks to represent the part-whole hierarchy in the data. What additionally contrasts our work with the follow-up works on capsule networks (Sabour et al., 2017;

Lenssen et al., 2018) is that our transformation coding is agnostic to the choice of architecture and training. We only rely on our objective function to enforce equivariance.

When considering the Euclidean group, our equivariant code produces a manifold that preserves distances in the embedding space under non-linear transformations of the input. This embedding should not be confused with isometric embedding (Tenenbaum et al., 2000), where the objective is to maintain the pairwise distances between points in the input and the embedding space.

3. Background on Symmetry Transformations

We can think of transformations as a set of bijective maps on a domain X , and since these maps are composable, we can identify their compositional structure using a group G . For this reason, such transformations are called group actions. To formally define transformation groups, we first define an abstract group. A *group* G is a set equipped with a binary operation, such that the set is closed under the operation $gg' \in G \forall g, g' \in G$, every $g \in G$ has a unique inverse such that $gg^{-1} = e$, where e is the identity element of the group, and the group operations are associative $(gg')g'' = g(g'g'')$.

A G -action on a set X is defined by a function $t : G \times X \rightarrow X$, which can be thought of as a bijective transformation parameterized by $g \in G$. In order to maintain the group structure, the action should satisfy the following two properties: (1) action of the identity is the identity transformation $t(e, x) = x$; (2) composition of two actions is equal to the action of the composition of group elements $t(g, t(g'x)) = t(gg', x)$. The action t is *faithful* to G if transformations of X using each $g \in G$ are unique – i.e., $\forall g, g' \exists x \in X$ s.t. $t(g, x) \neq t(g', x)$. If a G -action is defined on a set X , we call X a G -set.

4. Equivariance is Cheap, Actions Matter

A symmetry-based representation or embedding is a function $f : X \rightarrow Z$ such that both X and Z are G -sets, and furthermore f “knows about” G -actions, in the sense that transformations of the input using t_X have the same effect as transformations of the output using some action t_Z :

$$f(t_X(g, x)) = t_Z(f(x), g) \quad \forall g, x \in G \times X \quad (1)$$

The following claim shows that despite many efforts in designing equivariant networks, simply asking for the representation to be equivariant is not a strong inductive bias, and we argue that the action matters.

Proposition 4.1. *Given a transformation group $t_X : G \times X \rightarrow X$, the function $f : X \rightarrow Z$ is an equivariant representation if $\forall g \in G, x, x' \in X$*

$$f(x) = f(x') \Leftrightarrow f(t_X(g, x)) = f(t_X(g, x')). \quad (2)$$

That is, two embeddings are identical iff they are identical for all transformations.

The proof is in the appendix. The condition above is satisfied by all injective functions, indicating that many functions are equivariant to any group.

Corollary 4.2. Any injective function $f : X \rightarrow Z$ is equivariant to any transformation group $t_X : G \times X \rightarrow X$, if we define G action on the embedding space as

$$t_Z(g, z) \doteq f(t_X(g, f^{-1}(z))) \quad \forall g, z \in G \times Z \quad (3)$$

The ramification of the results above in what follows is two-fold:

1. While injectivity ensures equivariance, the group action on the embedding as shown in Equation (3) can become highly non-linear. Intuitively, this action recovers $x = f^{-1}(z)$, applies the group action $x' = t_X(x)$ in the input domains and maps back to the embedding space $f(x')$ to ensure equivariance. In the following, we push t_Z towards a simple linear G -action through optimization of f . This objective can be interpreted as a *symmetry regularization or a symmetry prior*.

2. Although Theorem 4.2 uses injectivity of f for the entire X , we only need this for the data manifold. In practice, one could enforce injectivity on the training dataset D using loss functions defined on the training data, for example, using a hinge loss (Hadsell et al., 2006)

$$L_{\text{hinge}}(f, D) = \sum_{x, x' \neq x \in D} \max(\epsilon - \|f(x) - f(x')\|, 0) \quad (4)$$

or other losses (barrier functions) that monotonically decrease with distance, such as $\frac{1}{\|f(x) - f(x')\|}$, or its logarithm $-\log(\|f(x) - f(x')\|)$. In experiments we use the logarithmic barrier function.

5. Symmetry Regularization Objectives

In learning equivariant representations, we often do not know the abstract group G and how it transforms our data, t_X . We assume that one can pick a reasonable abstract group G that “contains” the real abstract group acting on the data – *i.e.*, G action on the input may not be faithful. Our goal is to learn an $f : X \rightarrow Z$ that is equivariant w.r.t. the actions t_X, t_Z , where $t_X : X \times G \rightarrow X$ is unknown and t_Z is some (simple) G -action on Z of our choosing.

5.1. More Informed but Less Practical Setting

In the most informed case, the dataset also contains information about which group member $g \in G$ can be used to transform x to x' – that is the dataset consists of triples $(x, g, x_t = t_X(g, x))$. By having access to this information

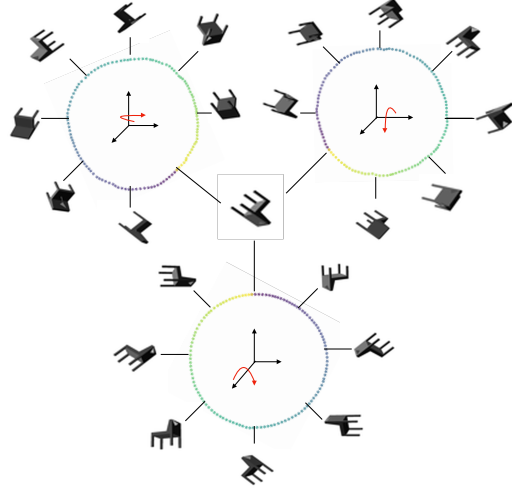


Figure 2. Visualization of the latent projection for the rotating Chair dataset. The chair is rotated in three orthogonal axis from 0 to 2π . The latent embedding for each pose of the chair is projected from 16D embedding space to a 2D space for visualization. The colors of the representations is mapped to the the angle of rotation of the chair. We notice that the mapping function f learnt is continuous with respect to the transformations of the object and it maps the rotations along an axis to a circular manifold. This is true for each orthogonal axis of rotation.

we can regularize the embedding using the following loss function:

$$L_G^{\text{informed}}(f, D) = \sum_{(x, g, x_t) \in D} \ell(f(x_t) - t_Z(g, f(x))) \quad (5)$$

where ℓ is an appropriate loss function such as the square loss. At its minimum, we have $f(x_t) = t_Z(g, f(x))$ or $f(t_X(g, x)) = t_Z(g, f(x))$, enforcing equivariance condition of Equation (1). However, even if the optimal value is not reach, due to its injectivity, f is still G -equivariant, and the the objective above is regularizing or simplifying the G action on the code.

The assumption of having access to g is often not realistic. As an example, in the Reinforcement Learning (RL) settings, where we have access to the action of the agent that can *transform* the state, although we have a triplet (x, a, x_t) , often a cannot be trivially mapped to a group element. Fortunately, using the fact that certain group actions are symmetries of some structures, we may still learn an equivariant embedding, even if we do not have the group information tied to the dataset. In this approach, the loss function and other potential sources of information in D will be group-specific. As we see shortly, for finite groups, we a symmetry regularization without any additional information is viable. However, for the remaining groups discussed in this paper, we need to be able to identify pairs of identical transformations – *i.e.*, transformations that use the “same”

group member – although we do not need to know the actual group member.

5.2. Finite Groups

Given two instances $x, x' \in D$, we may “optimize” for the choice of $g \in G$, such that $t_Z(f(x), g) \approx f(x')$, changing Equation (5) to

$$L_G(f, D) = \sum_{x, x' \in D} \min_{g \in G} \ell(f(x) - t_Z(g, f(x'))). \quad (6)$$

This approach may be suitable for finite groups, where one can enumerate $g \in G$ to perform the minimization inside the outer optimization. Since any finite group has a permutation representation, we can always define t_Z to permute blocks of the latent representation. In this case, the loss function above involves a search to find the best permutation within a group that matches the embeddings before and after the transformation.

For some permutation groups, this search can be performed more efficiently. For example, in the case of the symmetric group, the loss function of Equation (6) is also sometimes known as earth mover’s distance (Fan et al., 2017). One can also use the Chamfer distance to approximate this loss function. In contrast to the existing permutation equivariant networks (Zaheer et al., 2017; Qi et al., 2017), here the permutation action on the input is not limited to the permutation of a known group of variables – that is, the representation could be equivariant to shuffling of a priori unknown entities/objects in the input.

5.3. Euclidean Group

The defining action of the Euclidean group $E(n)$ is the set of transformations that preserve the Euclidean distance between any two points in \mathbb{R}^n , a.k.a. isometries. These transformations are compositions of translations, rotations, and reflections. Since for the real domain, all isometries are linear and belong to $E(n)$, we can enforce the group structure on the embedding by ensuring that distances between the embeddings before and after any transformation match. For this, we need the dataset D to be a set of pairs of pairs $((x, x_t = t_X(g, x)), (x', x'_t = t_X(g, x')))$, where x, x' are transformed using the same *unknown* group member g . Distance-preservation loss below combined with injection loss are sufficient to produce an $E(n)$ -regularized embedding:

$$L_{E(n)}(f, D) = \sum_{((x, x_t), (x', x'_t)) \in D} \ell \left(\overbrace{\|f(x) - f(x')\|}^{\text{distance before the transformation}} - \overbrace{\|f(x_t) - f(x'_t)\|}^{\text{distance after the transformation}} \right) \quad (7)$$

In the standard RL setup, where we have access to triplets

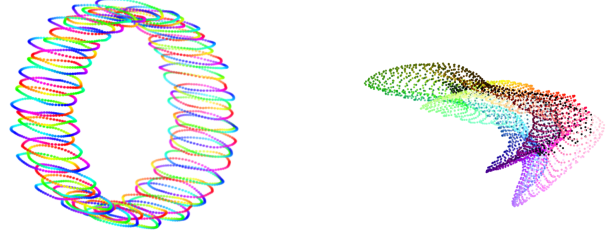


Figure 3. (left) Conformal vs. (right) VAE embedding of double-bump world.

(s, a, s') , we can easily form D by unrolling an episode and collecting two different state transitions corresponding to a particular action. In practice, with a finite actions, we can efficiently generate this dataset by keeping separate buffer for each action where we store state transitions for that action and sample from that buffer to train the embedding function f .

5.4. Orthogonal and Unitary Groups

The defining action of the orthogonal group $O(n)$ preserves the inner product between two vectors; these are exactly Euclidean isometries that fix the origin. The analogous group in the complex domain is the unitary group, which preserves the complex inner product. Our symmetry-regularization objective penalizes the change in the inner product of two embeddings before and after the same transformation:

$$L_{O(n)}(f, D) = \sum_{((x, x_t), (x', x'_t)) \in D} \ell(f(x)^\top f(x') - f(x_t)^\top f(x'_t)).$$

For the unitary group one additionally needs to embed to complex domain $Z = \mathbb{C}^n$ or use separate real and imaginary codes use the inner product of the complex domain.

5.5. Conformal Group

Conformal group is the group of transformations that preserve the angle. In a Euclidean embedding, these transformations include a combination of translation, rotation, dilation, and inversion with respect to an $n - 1$ -sphere. To enforce this group structure we need a triplets of inputs, before and after a transformation $((x, x_t), (x', x'_t), (x'', x''_t))$, so that we can calculate the angle in the embedding. Similar to distance-preserving loss of Equation (7), this objective enforces an *invariance*; this time we enforce the invariance of the angle between the triplet, before and the transformation:

$$L_{CO(n)}(f, D) = \sum_{((x, x_t), (x', x'_t), (x'', x''_t)) \in D} \ell \left(\cos(\angle f(x), f(x'), f(x'')) - \cos(\angle f(x'_t), f(x'_t), f(x''_t)) \right) \quad (8)$$

where $\cos(\angle y, y', y'') = \frac{(y-y')^\top (y''-y')}{\|y-y'\| \|y''-y'\|}$ is the cosine of the angle between the three embeddings.

This objective imposes a weaker constraint on the embedding than the distance preservation of the Euclidean group – preserving Euclidean distance implies preserving the angle. Moreover, it has an additional benefit that compared to $L_{E(n)}$ the loss cannot be minimized by simply shrinking the embedding, therefore in practice, the injection enforcing losses of Section 4 is no longer necessary when using conformal symmetry regularization.

6. Decomposing the Representation

Higgins et al. (2018) suggested a notion of disentangled representation based on decomposition of the abstract group into a direct product form $G = G_1 \times \dots \times G_k$. There are two approaches to learning such decomposed representation in transformation coding, depending on whether or not we can perform certain types of transformations in isolation. For example, an RL agent may transform its environment through actions like moving a single limb that can be performed in isolation. In this case, we call the decomposition *active* to contrast it with the *passive* case where the action of different subgroups is always mixed in our dataset.

6.1. Active Decomposition

Let $G = \{(g_1, \dots, g_k) \in G_1 \times \dots \times G_k\}$, where

$$G_i \cong \{(e, \dots, e, g_i, e, \dots, e) \in G\}$$

can be identified with a normal subgroup of G . In active decomposition, sub-groups can act in isolation and therefore we have k types of tuples in our dataset $D_1, \dots, D_k \subset D$. Each subset D_i is associated with actions of a subgroup G_i using $t_X((e, \dots, e, g_i, e, \dots, e), \cdot)$, $g_i \in G_i$.

In this setting, the representation $f : X \rightarrow Z = Z_1 \times \dots \times Z_k$ can be thought of as k separate functions where $f_i : X \rightarrow Z_i$ is equivariant to G_i -action and invariant to all $G_j, j \neq i$ actions. This gives the following objective

$$L_G^{\text{active}}(f, D) = \sum_{i=1}^k \underbrace{L_{G_i}(f_i, D_i)}_{\text{equivariance to } G_i} + \underbrace{L_{G/G_i}^{\text{inv.}}(f_i, D \setminus D_i)}_{\text{invariance to } G_j \text{ for } j \neq i} \quad (9)$$

where $L_G^{\text{inv.}}(f, D)$ enforces invariance of f to G -transformations in D – e.g., by penalizing $\|f(x) - f(t_X(g, x))\|$. In addition to isolated actions assumed in this setting we may have mixed actions. Moreover, if this mixing involves a known sparse subset of sub-groups (e.g., a subset of joints) the loss function of Equation (9) can be modified accordingly.

6.2. Passive Decomposition

When we have no control over transformations, and we are simply given the data, it is still possible to use an abstract group that has a product form. Here again, $f : X \rightarrow Z = Z_1 \times \dots \times Z_k$, but the loss function is simply enforced on each block separately – i.e., $L_G^{\text{passive}}(f, D) = \sum_{i=1}^k L_{G_i}(f_i, D)$, where $L_{G_i}(f_i, D)$ is a transformation coding objective from Section 5.

7. Experiments

We conducted many experiments to qualitatively study the representation learned by transformation coding, its ability to produce a disentangled representation, and quantitatively compare against simple baselines in both representation learning and downstream RL tasks. For details of architecture and training, see Appendix E.

7.1. Qualitative Analysis

In this section, we visualize the representation learned for two examples from the Gym environment (Brockman et al., 2016), including the pendulum and the mountain car (see Appendix B, followed by an experiment involving a rotating object where we know the ideal embedding in the form of $SO(3)$ manifold. Finally, Figure 3 visualizes a conformal embedding for double-bump world. In most cases we also visualize Variational AutoEncoder (VAE) (Kingma & Welling, 2013) embeddings for comparison. Our objective here is to visually demonstrate the behavior of transformation coding and its remarkable ability to learn embeddings that are informed by non-linear transformations of the input.



Figure 5. VAE embedding for the pendulum example; compare against Figure 1

7.1.1. THE PENDULUM

For this experiment, the input x is two consecutive frames of the pendulum that have been grayscaled and downsampled to 32×32 pixels. The action-space is a range of torques that can be applied on the base of the pendulum. We use the action to transform the data. We use the objective of Equation (7) to learn an $E(3)$ -equivariant representation. To efficiently estimate $L_{E(n)}$, we use a mini-batch that consists of 64 randomly sampled observations from the environment and their transformations via three randomly sampled actions (4×64 samples in total). Once the embedding $f(x)$ is produced, the pairwise distance between all 64^2 pairs is calculated, and the mini-batch loss penalizes the change in these distances between any pair of transformations in the mini-batch. Therefore, using this mini-batching procedure,

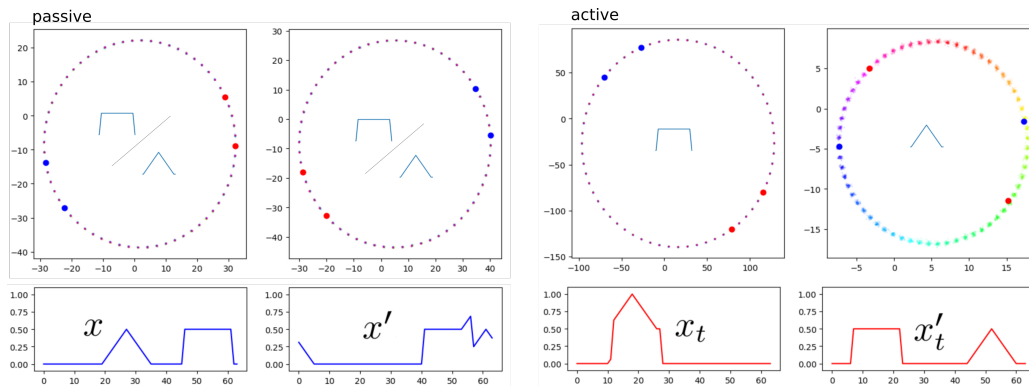


Figure 4. Active versus passive decomposition of the embedding for the double-bump world into $E(2) \times E(2)$ -set. In active decomposition (right), one of the manifolds encodes the circular translation of the triangle bump, while the second one represents the location of the square bump. Various colors indicate the location of the triangle. In the case of passive decomposition (left), since the decomposition is not guided by the transformation of individual shapes, the manifolds jointly encode the location of each bump type. The figure shows the embedding for two inputs before, (x, x') in blue, and after, (x_t, x'_t) in red, the *same* transformation. This transformation cyclically shifts both the triangle and the square to the left, but the amount of translation is larger for the square. In both passive and active decomposition, the Euclidean distance is preserved by the transformation – the red points have the same distance with each other as the blue points on every manifold.

the complexity of calculating the loss grows quadratically with both the number of independent samples and transformations.

The model on itself learns to parameterize the embedding using the location and the velocity of the pendulum from the input data; see Figure 1.¹ For comparison Figure 5 shows the embedding learned using a VAE from the same dataset. We perform a similar experiment in Mountain Car Environment and report its results in Appendix B.

7.1.2. ROTATING CHAIR

We consider a 3D chair from ModelNet40 (Wu et al., 2015) and transform it through the action of the group $SO(3)$. The group action in the input space is given by 2D projection into a 48×48 image after 3D rotation of the chair. While the group of interest is $SO(3)$, we use Euclidean regularization loss of Equation (7). In choosing the abstract group, we often only need to ensure that the group is large enough to contain the ground truth as a subgroup. Although this results in a stronger symmetry regularization on the embedding, a G -equivariant embedding is equivariant to any $H \leq G$. This means that, for example, an $E(2)$ equivariant embed-

¹A natural parametrization of a slow-moving pendulum using location and velocity is a cylinder, where the $SO(2)$ encodes the location, and \mathbb{R} encodes the velocity. At high velocities, the two ends of the cylinder twist and meet, forming a Klein bottle. However, the learned manifold of Figure 1 is different from both; it has a twist in the middle. This twist turns out to be necessary for enforcing $E(3)$ -equivariance. Because of the twist, the movement of the pendulum has the same direction around the circles on both sides. This is necessary for maintaining the distance of two points on opposite sides of the manifold after a transformation.

ding can be useful for its finite subgroups such as dihedral or cyclic groups. We embed the chair in \mathbb{R}^{16} using transformation coding² and visualize the latent by rotating the chair along three orthogonal axes and projecting the latent codes into a 2D space. Figure 2 shows three circular latent traversals corresponding to rotation around each axis, which is consistent with the structure of $SO(3)$ manifold. The process of learning $SO(3)$ manifold is a challenging task, and previous works assumed that the group member corresponding to each transformation is given (Quessard et al., 2020; Anonymous, 2022). In contrast, we only use the observations corresponding to similar actions during training and not the group members themselves. As we see later, this is critical in settings such as RL, where group information is unavailable. We were not able to produce a similar latent traversal for VAE due to collapse when rotating around some axes.

7.1.3. CONFORMAL GROUP FOR DOUBLE-BUMP WORLD

The double-bump world consists of a rectangular bump signal and a triangular bump signal, both of which have been cyclically shifted and superimposed. Any transformation in this dataset can be denoted as a pair (Δ_1, Δ_2) which cyclically shifts the rectangular bump by Δ_1 and the triangular bump by Δ_2 . In our experiments, the length of the signal is 64, and the length of the bump is 16. We used conformal loss of Equation (8) in this experiment. Figure 3(left)

²Note that while $SO(3)$ manifold is 3-dimensional, its isometric embedding requires a higher number of dimensions. Using a larger embedding dimension also often helps with the optimization of our symmetry regularization loss.

shows the random project of the embedding, where the colors change as the triangle bump moves. The figure suggests that transformation coding is able to successfully learn to represent a data point using the location of two bumps.

7.2. Experiments on Active and Passive Decomposition

In this section, we first contrast active and passive decomposition in their ability to disentangle the two bumps in the double bump world. We observe that while both can decompose the embedding into a product form $SO(2) \times SO(2)$, only active decomposition leads to disentanglement. Section 7.2.2 applies active decomposition to a more complex setting of ego-motion, where transformation coding can decompose the representation of the agent’s state into location and orientation.

7.2.1. DECOMPOSITION OF THE DOUBLE-BUMP WORLD

Next, we compare the active and passive decomposition for the same double-bump world. While the ground truth is $SO(2) \times SO(2)$, the method uses the larger group $E(2) \times E(2)$. In the active case, each subgroup moves one of the bumps, the loss of Equation (9) is used to learn an embedding for each subgroup. In the passive case, both bumps move randomly.

Figure 4 compares the decomposed embedding found in each case. While in both cases, the $SO(2) \times SO(2)$ torus is decomposed into a product of circles, only the active case successfully disentangles the two bumps. Note that the color of each point is based on the location of the triangle bump. Our results agree with Caselles-Dupré et al. (2019) who claim that learning a disentangled representation requires interaction with the environment; see also (Painter et al., 2020; Mita et al., 2021). However, we note that while the disentangling of the bump movements do not happen in the passive case, we can still successfully “decompose” the embedding.

7.2.2. ACTIVE DECOMPOSITION FOR EGO-MOTION

We used a modified version of the single-room environment of Mini-World (Chevalier-Boisvert, 2018) for this experiment. The agent is standing in a 3D room containing eight differently colored boxes around the walls. A map of the room can be seen in Figure 7. An observation consists of a first-person view of the room, downsampled to 32×32 pixels. The agent can rotate left/right or move forward/backward. We learn an $E(2) \times E(2)$ equivariant embedding using the active decomposition objective of Equation (9). Each mini-batch consists of 64 random observations and the result of applying all four actions in

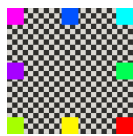


Figure 7. Top view of the room

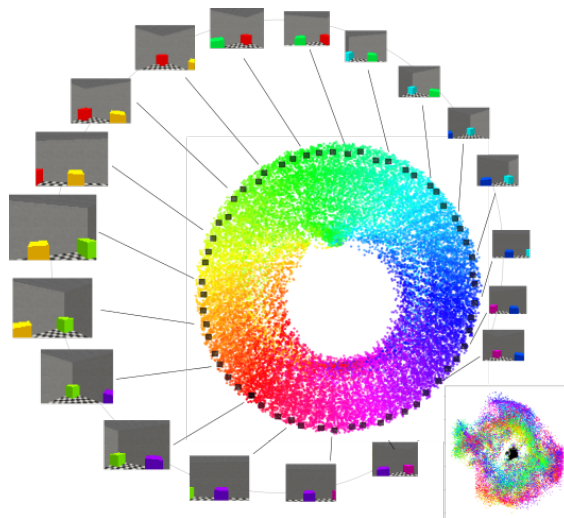


Figure 6. Decomposition of the ego-motion manifold using $E(2) \times E(2)$ equivariant coding. The dataset contains a first-person view of a room. Transformations include right-left rotation and forward-backward movement. The equivariant embedding is produced by active decomposition using these two transformations, where the ring-structured manifold corresponds to the rotation action, and the smaller manifold corresponds to translations. Color-coding shows the true angle of the image. The black square markers show the traversal of the embedding as the agent rotates while standing in the middle of the room. Note that in the second manifold, black squares are concentrated in the center.

those states (4×64 samples in total).

Figure 6 visualizes the embedding of the input in two sub-figures, where the more prominent figure shows the embedding corresponding to the rotation action, and the more petite figure (bottom right) shows the embedding corresponding to forward-backward movement. The first figure also shows the first-person view when the agent rotates while standing in the middle of the room. The corresponding markers collapse around the center of the second embedding, demonstrating an intuitive embedding, parameterized by rotation angle and location. Walking straight across the room also produces the expected behavior of traversing the second manifold while the rotation angle, for the most part, remains fixed (not shown).

7.3. Quantitative Evaluation in Downstream Tasks

This section quantitatively shows the effectiveness of transformation coding for World Modelling and RL.

7.3.1. WORLD MODELLING

We select Atari games Pong and Space Invader for the world modeling experiments as our environment. These environments are previously used by (Kipf et al., 2020) to evaluate

Table 1. Hits at Rank 1 (H@1) and Mean Reciprocal Rank (MRR) of different method. We report our models performance over 5 random seeds for Pong and Space Invaders.

ENVIRONMENT	METHOD	H@1	MRR
ATARI PONG	WORLD MODEL(AE)	23.8 \pm 3.3	44.7 \pm 2.4
	WORLD MODEL(VAE)	1.0 \pm 0.0	5.1 \pm 0.1
	C-SWM	36.5 \pm 5.6	56.2 \pm 6.2
	Ours	45.2\pm 3.4	60.2\pm 3.9
SPACE INVADERS	WORLD MODEL(AE)	40.2 \pm 3.3	59.6 \pm 3.5
	WORLD MODEL(VAE)	1.0 \pm 5.3	5.3 \pm 0.1
	C-SWM	48.5 \pm 7.0	66.1 \pm 6.6
	Ours	54.2\pm 6.3	68.7\pm 5.1

their model, Contrastive Structured World Model (C-SWM). We train the encoder using our Euclidean transformation coding objective, freeze it, and then learn a Multi-Layer Perceptron (MLP) based transition function in the latent space. Our evaluation scheme follows (Kipf et al., 2020). We report Hits at Rank 1 (H@1) and Mean Reciprocal Rank (MRR), which are invariant to the embedding scale. These evaluation metrics measure the relative closeness of the next state’s representation predicted by the transition model and the representation of the observed next state. To measure the relative closeness, we use a set of reference state representations (embedding of random observations from the experience buffer). Table 1 reports these measures and show that a simple transition model learned on top of our embedding outperforms C-SWM in both games. Other reported baselines use an AutoEncoder (AE) and a Variational AutoEncoder (VAE) to learn embeddings.

7.3.2. REINFORCEMENT LEARNING

Next, we consider three Mujoco environments: InvertedPendulum, Reacher, and Swimmer from OpenAI Gym (Brockman et al., 2016). We introduce two variations of our model to test the usefulness of transformation coding in the context of RL. The first variation uses a fixed encoder that is pretrained using transformation coding and then trains an MLP heads for function approximations in the downstream RL algorithm (TC-decoupled); that is, the low-dimensional embedding is used as a substitute for the high-dimensional input data without further adjustment. The second variation allows for finetuning during the reinforcement learning stage (TC-finetuned). We designed two other baseline models using AutoEncoder (AE) to train the encoder and call them AE-decoupled and AE-finetuned. We use Proximal Policy Optimization (PPO) (Schulman et al., 2017) as the underlying RL algorithm. To evaluate the data-efficiency of these models, we report the average reward collected over 10 episodes in the first 100,000 steps for Reacher and Swimmer and 30,000 steps for Inverted Pendulum in Table 2 (since Inverted Pendulum generally learns faster, we took a fewer number of steps.)

Table 2. Average reward collected over 10 episodes for various models in Inverted Pendulum, Reacher and Swimmer. We provide the standard error for each of them using 5 different random seeds for each experiment.

METHODS	INVERTEDPENDULUM	REACHER	SWIMMER
VANILLA	500 \pm 150	-11 \pm 2.5	25.6 \pm 3.4
AE-DECOUPLED	30 \pm 15	-13 \pm 3.0	16 \pm 3.9
AE-FINETUNED	580 \pm 130	-11.5 \pm 3.2	26 \pm 4.3
TC-DECOUPLED	800 \pm 180	-14.5 \pm 3.1	21 \pm 4.1
TC-FINETUNED	950\pm 50	-10\pm 3.4	31.5\pm 3.9

We see that learned representations adequately capture the structure of the environment in Inverted Pendulum since the RL agent just trained on the fixed representation (TC-decoupled) outperforms vanilla PPO. In contrast, AE does not seem to capture the structure, at least not in a form suitable for learning a policy. In Reacher, TC-decoupled performs poorly compared to AE-decoupled. We believe that this is because the representation is focused on transformations due to the agent’s actions, and details that can be valuable from the reward’s perspective can be ignored – in this case, the small object that the Reacher should reach. This observation points to a significant limitation of our approach, that is in this case resolved by finetuning. Like Reacher, we see that learning the agent’s transformations is not enough to get all the reward information as the background movement decides how far the agent has swum. Indeed, allowing the encoder to finetune allows the representations to reflect the reward information and improve performance.

Conclusion

Transformation coding is shown to be a simple, intuitive, and yet effective approach for learning equivariant representations, where the group action on the input is potentially non-linear and unknown. The idea is to learn a bijection that is regularized towards simple actions of the abstract group on the latent space. Symmetry regularization loss is specific to each group and relies on the preservation of certain quantities. This is reminiscent of the unification of geometries using group theory in Klein’s Erlangen program; preservation of distance, inner product, and angle are used to define latent representations equivariant to Euclidean, orthonormal, and conformal groups. This also points to an important limitation: a recipe for creating symmetry regularization losses for general Lie groups is currently missing. While this paper showcases the effectiveness of transformation coding in several qualitative and quantitative experiments, we see many avenues for further exploration in future works.

References

- Anonymous. Learning symmetric representations for equivariant world models. In *Submitted to The Tenth International Conference on Learning Representations*, 2022. URL <https://openreview.net/forum?id=D637S6zBRLD>. under review.
- Bengio, Y., Courville, A., and Vincent, P. Representation learning: A review and new perspectives. *IEEE transactions on pattern analysis and machine intelligence*, 35(8): 1798–1828, 2013.
- Brockman, G., Cheung, V., Pettersson, L., Schneider, J., Schulman, J., Tang, J., and Zaremba, W. Openai gym. *arXiv preprint arXiv:1606.01540*, 2016.
- Burgess, C. P., Higgins, I., Pal, A., Matthey, L., Watters, N., Desjardins, G., and Lerchner, A. Understanding disentangling in beta-vae. *arXiv preprint arXiv:1804.03599*, 2018.
- Caselles-Dupré, H., Garcia-Ortiz, M., and Filliat, D. Symmetry-based disentangled representation learning requires interaction with environments. *arXiv preprint arXiv:1904.00243*, 2019.
- Chen, T., Kornblith, S., Norouzi, M., and Hinton, G. A simple framework for contrastive learning of visual representations. In *International conference on machine learning*, pp. 1597–1607. PMLR, 2020.
- Chen, X., Duan, Y., Houthoofd, R., Schulman, J., Sutskever, I., and Abbeel, P. Infogan: Interpretable representation learning by information maximizing generative adversarial nets. *arXiv preprint arXiv:1606.03657*, 2016.
- Chevalier-Boisvert, M. gym-miniworld environment for openai gym. <https://github.com/maximecb/gym-miniworld>, 2018.
- Cohen, T. and Welling, M. Group equivariant convolutional networks. In *International conference on machine learning*, pp. 2990–2999. PMLR, 2016.
- Cohen, T. S. and Welling, M. Transformation properties of learned visual representations. *arXiv preprint arXiv:1412.7659*, 2014.
- Cohen, T. S., Geiger, M., and Weiler, M. A general theory of equivariant CNNs on homogeneous spaces. In Wallach, H., Larochelle, H., Beygelzimer, A., d’Alché-Buc, F., Fox, E., and Garnett, R. (eds.), *Advances in Neural Information Processing Systems*, volume 32, pp. 9145–9156. Curran Associates, Inc., 2019. URL <https://proceedings.neurips.cc/paper/2019/file/b9cfe8b6042cf759dc4c0cccb27a6737-Paper.pdf>.
- Ermolov, A., Siarohin, A., Sangineto, E., and Sebe, N. Whitening for self-supervised representation learning. In *International Conference on Machine Learning*, pp. 3015–3024. PMLR, 2021.
- Falorsi, L., de Haan, P., Davidson, T. R., De Cao, N., Weiler, M., Forré, P., and Cohen, T. S. Explorations in homeomorphic variational auto-encoding. *arXiv preprint arXiv:1807.04689*, 2018.
- Fan, H., Su, H., and Guibas, L. J. A point set generation network for 3d object reconstruction from a single image. In *Proceedings of the IEEE conference on computer vision and pattern recognition*, pp. 605–613, 2017.
- Finzi, M., Welling, M., and Wilson, A. G. A practical method for constructing equivariant multilayer perceptrons for arbitrary matrix groups. *arXiv preprint arXiv:2104.09459*, 2021.
- Hadsell, R., Chopra, S., and LeCun, Y. Dimensionality reduction by learning an invariant mapping. In *2006 IEEE Computer Society Conference on Computer Vision and Pattern Recognition (CVPR’06)*, volume 2, pp. 1735–1742. IEEE, 2006.
- He, K., Fan, H., Wu, Y., Xie, S., and Girshick, R. Momentum contrast for unsupervised visual representation learning. In *Proceedings of the IEEE/CVF Conference on Computer Vision and Pattern Recognition*, pp. 9729–9738, 2020.
- Higgins, I., Amos, D., Pfau, D., Racaniere, S., Matthey, L., Rezende, D., and Lerchner, A. Towards a definition of disentangled representations. *arXiv preprint arXiv:1812.02230*, 2018.
- Hinton, G. E., Krizhevsky, A., and Wang, S. D. Transforming auto-encoders. In *International conference on artificial neural networks*, pp. 44–51. Springer, 2011.
- Kingma, D. P. and Welling, M. Auto-encoding variational bayes. *arXiv preprint arXiv:1312.6114*, 2013.
- Kipf, T., van der Pol, E., and Welling, M. Contrastive learning of structured world models. In *International Conference on Learning Representations*, 2020. URL <https://openreview.net/forum?id=Hlgax6VtDB>.
- Kondor, R. and Trivedi, S. On the generalization of equivariance and convolution in neural networks to the action of compact groups. In *International Conference on Machine Learning*, pp. 2747–2755. PMLR, 2018.
- Kulkarni, T. D., Whitney, W., Kohli, P., and Tenenbaum, J. B. Deep convolutional inverse graphics network. *arXiv preprint arXiv:1503.03167*, 2015.

- Langley, P. Crafting papers on machine learning. In Langley, P. (ed.), *Proceedings of the 17th International Conference on Machine Learning (ICML 2000)*, pp. 1207–1216, Stanford, CA, 2000. Morgan Kaufmann.
- Lenc, K. and Vedaldi, A. Learning covariant feature detectors. In *European conference on computer vision*, pp. 100–117. Springer, 2016.
- Lenssen, J. E., Fey, M., and Libuschewski, P. Group equivariant capsule networks. In Bengio, S., Wallach, H., Larochelle, H., Grauman, K., Cesa-Bianchi, N., and Garnett, R. (eds.), *Advances in Neural Information Processing Systems*, volume 31, pp. 8844–8853. Curran Associates, Inc., 2018. URL <https://proceedings.neurips.cc/paper/2018/file/c7d0e7e2922845f3e1185d246d01365d-Paper.pdf>.
- Mita, G., Filippone, M., and Michiardi, P. An identifiable double vae for disentangled representations. In *International Conference on Machine Learning*, pp. 7769–7779. PMLR, 2021.
- Oord, A. v. d., Li, Y., and Vinyals, O. Representation learning with contrastive predictive coding. *arXiv preprint arXiv:1807.03748*, 2018.
- Painter, M., Hare, J., and Prugel-Bennett, A. Linear disentangled representations and unsupervised action estimation. *arXiv preprint arXiv:2008.07922*, 2020.
- Qi, C. R., Su, H., Mo, K., and Guibas, L. J. Pointnet: Deep learning on point sets for 3D classification and segmentation. In *Proceedings of the IEEE conference on computer vision and pattern recognition*, pp. 652–660, 2017.
- Quessard, R., Barrett, T. D., and Clements, W. R. Learning group structure and disentangled representations of dynamical environments. *arXiv preprint arXiv:2002.06991*, 2020.
- Raffin, A., Hill, A., Gleave, A., Kanervisto, A., Ernestus, M., and Dormann, N. Stable-baselines3: Reliable reinforcement learning implementations. *Journal of Machine Learning Research*, 22(268):1–8, 2021. URL <http://jmlr.org/papers/v22/20-1364.html>.
- Ravanbakhsh, S., Schneider, J., and Póczos, B. Equivariance through parameter-sharing. In *International Conference on Machine Learning*, pp. 2892–2901. PMLR, 2017.
- Sabour, S., Frosst, N., and Hinton, G. E. Dynamic routing between capsules. In Guyon, I., Luxburg, U. V., Bengio, S., Wallach, H., Fergus, R., Vishwanathan, S., and Garnett, R. (eds.), *Advances in Neural Information Processing Systems*, volume 30, pp. 3856–3866. Curran Associates, Inc., 2017. URL <https://proceedings.neurips.cc/paper/2017/file/2cad8fa47bbef282badbb8de5374b894-Paper.pdf>.
- Schulman, J., Wolski, F., Dhariwal, P., Radford, A., and Klimov, O. Proximal policy optimization algorithms, 2017.
- Tenenbaum, J. B., De Silva, V., and Langford, J. C. A global geometric framework for nonlinear dimensionality reduction. *science*, 290(5500):2319–2323, 2000.
- Tian, Y., Krishnan, D., and Isola, P. Contrastive multiview coding. *arXiv preprint arXiv:1906.05849*, 2019.
- Villar, S., Hogg, D., Storey-Fisher, K., Yao, W., and Blum-Smith, B. Scalars are universal: Equivariant machine learning, structured like classical physics. *Advances in Neural Information Processing Systems*, 34, 2021.
- Wood, J. and Shawe-Taylor, J. Representation theory and invariant neural networks. *Discrete applied mathematics*, 69(1-2):33–60, 1996.
- Worrall, D. E., Garbin, S. J., Turmukhambetov, D., and Brostow, G. J. Interpretable transformations with encoder-decoder networks. In *Proceedings of the IEEE International Conference on Computer Vision*, pp. 5726–5735, 2017.
- Wu, Z., Song, S., Khosla, A., Yu, F., Zhang, L., Tang, X., and Xiao, J. 3d shapenets: A deep representation for volumetric shapes. In *Proceedings of the IEEE conference on computer vision and pattern recognition*, pp. 1912–1920, 2015.
- Zaheer, M., Kottur, S., Ravanbakhsh, S., Póczos, B., Salakhutdinov, R. R., and Smola, A. J. Deep sets. In Guyon, I., Luxburg, U. V., Bengio, S., Wallach, H., Fergus, R., Vishwanathan, S., and Garnett, R. (eds.), *Advances in Neural Information Processing Systems*, volume 30, pp. 3391–3401. Curran Associates, Inc., 2017. URL <https://proceedings.neurips.cc/paper/2017/file/f22e4747dalaa27e363d86d40ff442fe-Paper.pdf>.
- Zbontar, J., Jing, L., Misra, I., LeCun, Y., and Deny, S. Barlow twins: Self-supervised learning via redundancy reduction. *arXiv preprint arXiv:2103.03230*, 2021.

A. Proof of Claims

Proof. of Claim 1

Let \sim_f be an equivalence relation on X , such that two points are “equivalent” if they have the same embedding $x \sim x' \Leftrightarrow f(x) = f(x')$. We use $[x]_{\sim}$ to denote the equivalence class of x . To get an intuition for this result, first consider an injective f , where the equivalence classes are trivial $[x]_{\sim} = x$. In this case for any G -set X , f is G -equivariant with G -action on Z defined by

$$t_Z(g, y) \doteq f(t_X(g, f^{-1}(y))) \quad \forall g, y \in G \times Z \quad (10)$$

Now to see why f is equivariant to any action t_X and the corresponding t_Z defined above, simply replace the definition of t_Z into definition of equivariance Equation (1)

$$t_Z(g, f(x)) = f(t_X(g, f^{-1}(f(x)))) = f(t_X(g, x)) \quad (11)$$

For general functions, note that $f^{-1}(f(x)) = [x]_{\sim}$. The equation above makes sense iff $t_X(g, x') = t_X(g, x'') \forall x', x'' \in [x]_{\sim}$, which is basically the assumption of Equation (2). This means $[t_X(g, x)]_{\sim} \doteq [t_X(g, x)]_{\sim}$, and using the t_Z of Equation (10) in the definition of equivariance, we see that its condition is satisfied

$$t_Z(g, f(x)) = f(t_X(g, f^{-1}(f(x)))) = f(t_X(g, [x]_{\sim})) = f([t_X(g, x)]_{\sim}) = f(t_X(g, x)) \quad (12)$$

□

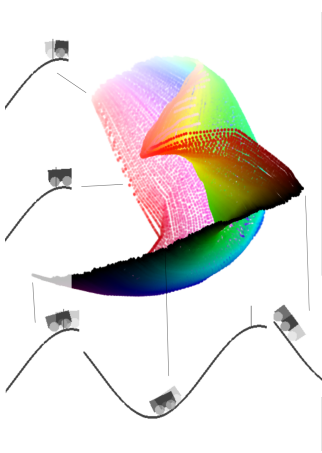


Figure 8. The $E(3)$ equivariant representation of the mountain-car. Each state $x \in X$ is a concatenation of two consecutive frames so as to inform about both position and velocity of the car. The colors encode the true position of the car, and the brightness of the colors shows the positive-negative velocity. The transformation $t_X(g, x)$ changes the velocity through positive/negative acceleration. By preserving the distance between pairs of instances in which the same acceleration is applied, transformation coding is able to recover a manifold that is parameters by velocity and location.

B. Additional Experiment: the Mountain Car

In the Mountain Car environment, an observation x consists of two consecutive frames that have been grayscaled and downsampled to 32×32 pixels. The action-space of the environment is a range of accelerations that can be applied to the car. Figure 8 shows the learned embedding in \mathbb{R}^3 . Figure 8 shows the learned embedding in \mathbb{R}^3 . Colors show the change in the location and the brightness shows the velocity. The learned representation is quite intuitive, and the model learns to parameterize the manifold using the location and velocity of the car.

C. Addition of Invariant Features

While we focused on equivariant codes, one may also consider an invariant component in the code which can account for variations in the data that are not due to transformations – that is, we have $f : X \rightarrow Z \times Y$, where Y is the invariant part of the code that identifies distinct *orbits*. Let $f^{\text{inv.}} : X \rightarrow Y$ denote the invariant component of f . To learn $f^{\text{inv.}}$, one could use a loss of the form $\ell(f^{\text{inv.}}(x) - f^{\text{inv.}}(t_X(g, x)))$ which enforces invariance for points on the same orbit. At the same time, an injection loss, similar to those of Section 4, pushes apart the points that are not in the same orbit. This invariant component is therefore very similar to what is used in contrastive coding.



Figure 9. VAE embedding for the Mountain Car example; compare against Figure 8

D. Effect of Transformations on the Embedding Manifold

When using transformation coding, the transformation can have a complex relationship with the ideal parameterizations of the manifold. For example, the location and velocity of the mountain-car or the pendulum (as ideal parameters for the manifold), are non-trivially related to the action that accelerates the movement. A natural question here is about the effect of the choice of transformation on the manifold. In practice, we observe that, in low-dimensional embedding, the geometry of the manifold is quite sensitive to the choice of transformation. As an example, Figure 10 presents an alternative embedding for the pendulum of Figure 1 obtained by simply decreasing the amount of time between taking an action, and observing its outcome from $\delta t = .05 \rightarrow \delta t = .01$. Whether or not this (potential) sensitivity is a bug or feature may depend on the application setting.

E. Implementation Details

Pendulum and Mountain Car We use the same setting for both of these environments. The neural network first applies three convolutional layers with 3×3 kernels, 24 output channels, and “same” padding, each followed by 2×2 max pooling and ReLU activation. Finally, a Multi-Layer Perceptron (MLP) with a single hidden layer of size 128 and ReLU activation is applied to embed the representation into \mathbb{R}^3 . The model was trained for 5000 steps with the Adam optimizer set to a learning rate of 10^{-3} . The log-barrier coefficient was set to 1, and we used a weight decay coefficient of 10^{-7} .

Bump World The neural network used for conformal coding experiments in Section 7.1.3 is a 4-layer MLP with hidden layers of size 128 and ReLU activation functions. The embedding space is \mathbb{R}^4 which is then randomly projected to \mathbb{R}^3 for visualization. The log-barrier coefficient and weight decay coefficient were both set to 10^{-7} . The mini-batches used for training consist of 64 randomly sampled observations from the environment and their transformations via 15 randomly sampled transformations (16×64 samples in total). The model was trained for 10,000 steps with the Adam optimizer set to a learning rate of 10^{-3} .

The neural network used in active and passive decomposition experiments in Section 7.2.1 is a 3-layer MLP with hidden layers of size 128 and ELU activation functions. The embedding space is \mathbb{R}^4 which we interpret as two \mathbb{R}^2 s. We optimize the model for 5000 steps using the Adam optimizer with an initial learning rate of 10^{-2} which is halved every 1000. We use a barrier coefficient of 1 and a weight decay coefficient of 10^{-5} . The mini-batches used for training consist of 64 randomly sampled observations from the environment and their transformations via 7 randomly sampled transformations (8×64 samples in total).

Gym Mini-world The neural network architecture and training settings are similar to those of the pendulum and mountain car experiments.

Rotating chair The neural network used for the Chair dataset first applies three convolutional layers with 3×3 kernels, increasing number of output channels from 16 to 32 to 64, 1 padding and stride of 2. It is followed by a ReLU activation. Finally, a Multi-Layer Perceptron (MLP) with a single hidden layer of size 128 and ReLU activation is applied to embed the representation into \mathbb{R}^{16} . The model was trained with 10000 unique rotations repeated with multiple initial points with the Adam optimizer set to a learning rate of 10^{-3} . We stick to small rotation angles to make the setup similar to dynamical environments. The log-barrier loss coefficient was set to 1, and we used a weight decay coefficient of 10^{-7} .

Pong and Space Invaders The neural network used for the Chair dataset first applies three convolutional layers with 7×7 , 5×5 and 3×3 kernels. We again increase the number of output channels from 16 to 32 to 64 and use a padding of 1 and stride of 2 for all of them. The convolutions are followed by ReLU activations. Finally, a linear layer is applied to embed the representation into \mathbb{R}^{32} . We train the encoder with samples collected from around 100k environment steps. The log-barrier loss coefficient was again set to 1.

Pendulum, Reacher and Swimmer The encoder and pre-training setting used for this part is similar to the one used for Pong and space invaders. We use an MLP to learn the policy from the extracted features. We use stable baselines 3 for our PPO implementation. (Raffin et al., 2021).

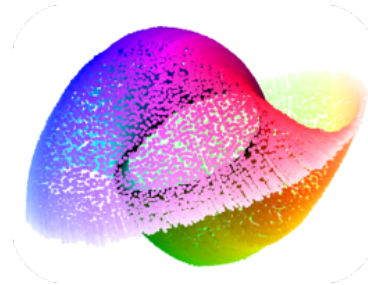


Figure 10. Alternative embedding for the pendulum.